International Journal of Biological Macromolecules 245 (2023) 125459

Contents lists available at ScienceDirect

International Journal of Biological Macromolecules

journal homepage: www.elsevier.com/locate/ijbiomac

Integrated multiomics analysis reveals changes in liver physiological function in *Aqp9* gene knockout mice

Quancheng Cheng [a,1], Junwei Zhang [b,1], Huiru Ding [a], Ziyuan Wang [a], Jinyu Fang [a], Xuan Fang [a,1], Man Li [a], Rui Li [c], Jieyi Meng [a], Huaicun Liu [a], Xin Lu [b], Yiyao Xu [b], Chunhua Chen [a,*], Weiguang Zhang [a,*]

[a] Department of Human Anatomy and Histology and Embryology, School of Basic Medical Sciences, Peking University Health Science Center, Beijing 100191, China
[b] Department of Liver Surgery, State Key Laboratory of Complex Severe and Rare Diseases, Peking Union Medical College (PUMC) Hospital, Chinese Academy of Medical Sciences and Peking Union Medical College, Beijing 100730, China
[c] Department of Otolaryngology Head and Neck Surgery, Peking University Third Hospital, Beijing 100191, China

ARTICLE INFO

Keywords:
Aquaporin 9
Immune
Inflammation
Cathepsin S
CD4

ABSTRACT

Aquaporin 9 (AQP9) is the main channel by which blood glycerol enters the liver, where it plays key roles in osmotic pressure regulation and energy metabolism. Previous studies have shown that AQP9 is involved in the pathogenesis of many liver diseases. In this study, we aimed to clarify the role of AQP9 in maintaining the physiological environment of the liver using $Aqp9^{-/-}$ mice. We constructed *Aqp9* knockout mice and used comprehensive multiomics analysis to elucidate the potential molecular effects of AQP9 expression on liver tissue. Knockout of *Aqp9* reduced mouse body weight by affecting glycerol metabolism and led to hepatocyte death and inflammatory cell infiltration, which was confirmed by transcriptomics, proteomics and metabolomics. Moreover, knockout of *Aqp9* triggered immune and inflammatory responses, leading to scattered and mild liver cell pyroptosis and compensatory liver cell proliferation.

1. Introduction

Aquaporins (AQPs) are channel proteins located in the membrane that mainly regulate the water flow between cells. To date, 13 kinds of AQPs have been found in mammals, and they are widely distributed in specific cell types in various organs and tissues [1]. AQPs can be divided into 3 subfamilies [2]: classic AQPs, aquaglyceroporins and nonclassical AQPs. Aquaporin 9 (AQP9), an aquaglyceroporin channel protein, is the main channel by which blood glycerol enters the liver, and it plays a key role in osmotic pressure regulation and energy metabolism [3]. It can also transport some small molecular solutes, including monocarboxylic acid (such as lactic acid), glycerin, urea, purine, pyrimidine and H_2O_2 [4].

As a result of its functional diversity in the liver, AQP9 is involved in the pathogenesis of many liver-related diseases. Most studies have shown that the expression of AQP9 is positively correlated to the severity of fatty liver disease [4–6]. Studies have confirmed that downregulating the expression of AQP9 can alleviate oleic acid-induced steatosis in an in vitro cell model [7]. Other studies have shown that the expression of AQP9 in the liver is downregulated in nonalcoholic fatty liver disease (NAFLD) models and obese patients with T2D [8,9]. In an oleic acid-induced NAFLD cell model, the mRNA level of AQP9 was not significantly changed, but its protein expression was downregulated. The expression level of AQP9 increased after lipid-lowering drug intervention [10]. Our previous study demonstrated that AQP9 is involved in chronic liver injury and that knockout of AQP9 effectively counteracts the progression of chronic liver injury [11]. From the perspective of AQP9's participation in gluconeogenesis, the glycerol permeability of AQP9 is directly proportional to its expression level, and it maximizes liver glycerol import during states requiring increased glucose

Abbreviations: AQPs, aquaporins; AQP9, aquaporin 9; NAFLD, nonalcoholic fatty liver disease; WT, wild-type; KO, knockout; HFD, high-fat diet; PVL, portal vein ligation; TG, triglyceride; HE, hematoxylin and eosin; IHC, immunohistochemistry; DEGs, differentially expressed genes; Ctss, cathepsin S; DEPs, differentially expressed proteins; cAMP, cyclic adenosine monophosphate; MHC-II, major histocompatibility complex class II.

* Corresponding authors at: Department of Human Anatomy and Histology and Embryology, School of Basic Medical Sciences, Peking University, Beijing 100191, China.
E-mail addresses: cch@bjmu.edu.cn (C. Chen), zhangwg@bjmu.edu.cn (W. Zhang).
[1] These authors contributed equally.

https://doi.org/10.1016/j.ijbiomac.2023.125459
Received 16 December 2022; Received in revised form 22 May 2023; Accepted 10 June 2023
Available online 21 June 2023

production [12]. AQP9 has also been reported to be involved in energy metabolism during liver regeneration after hepatectomy by promoting gluconeogenesis [13]. AQP9 plays a variety of role in different diseases or even different stages of the same disease. Therefore, it is important to clarify the role of AQP9 in maintaining the physiological environment of the liver under basal conditions. This investigation will help deepen the understanding of the role and underlying molecular mechanisms of AQP9 in various liver diseases.

Omics research techniques are helpful for investigating comprehensive changes at the RNA, protein and metabolic levels. Omics has been used to explore the molecular mechanisms of many diseases. However, single-omics-based techniques are limited by providing only one-dimensional changes in the expression of biomolecules (such as mRNA, proteins, and metabolites), hindering a comprehensive understanding of molecular mechanisms and the identification of molecular initiation events and critical events in the pathogenesis of a disease. To overcome these challenges, multiomics approaches using at least two or more omics techniques are recommended [14]. The integration of multiomics allows us to effectively capture the multifaceted network from gene to phenotype and understand a range of molecular mechanisms [15]. Comprehensive multiomics analysis can help to more fully elucidate the potential molecular mechanisms involving AQP9 in liver tissue.

In this study, we constructed *Aqp9* knockout mice and used transcriptomics, proteomics and metabolomics to screen the AQP9-related molecular pathways in the physiological basal state. Through experimental verification, it was confirmed that *Aqp9* knockout could trigger immune and inflammatory responses, causing scattered mild pyroptosis of liver cells, which led to compensatory liver cell proliferation.

2. Methods

2.1. Ethics statement

All animal experiments were reviewed and approved by the Biomedical Ethics Committee of the Peking University Institutional Review Board (No. LA2017100) and performed following the Chinese national guidelines for the care of laboratory animals. All efforts were made to minimize suffering. The animals were housed in individual cages under controlled humidity, temperature and light (12 h light/12 h dark cycle). Food and water were available ad libitum.

2.2. Building animal models

Aqp9$^{-/-}$ mice were supplied by Peking University, and their model construction method was performed as previously described [11]. Wild-type (WT) mice (C57BL/6) were purchased from the Peking University Health Science Center Department of Laboratory Animal Science. The mice were deeply anesthetized with isoflurane and then sacrificed. For all experiments, a minimal number of animals were used, and pain was minimized to the best extent possible. As shown in Fig. S1 (Supplementary document 1), three animal models were used in this study. All animals were prevented from eating or drinking the night before sacrifice.

2.2.1. Normal physiological state model

Sixteen mice (male) were divided into the WT (wild-type) group and KO (knockout) group. All mice weighed approximately 20–25 g (5–6 weeks) and were fed a normal diet for the next 10 weeks. Their body weight was measured weekly.

2.2.2. NAFLD

Sixteen mice (male) were divided into the WT-Control group and WT-HFD (high-fat diet) group, which were fed the control diet and HFD, respectively, for 12 weeks. The control diet (D12450K, Research Diets, NJ, USA) was composed of 10 % fat-derived calories, while the HFD (D12492, Research Diets, NJ, USA) had 60 % fat-derived calories. All mice were fed a normal diet for 6 weeks until they weighed approximately 22 g, followed by the assigned diet for the next 12 weeks. Their body weight was measured weekly.

2.2.3. Portal vein ligation (PVL)

Sixteen mice (male) were divided into the WT-Control group and the WT-PVL group. All mice weighed approximately 20–25 g (5–6 weeks). For the WT-PVL group, the left branch of the portal vein, which feeds into the middle liver lobe, left lateral liver lobe and caudate liver lobe, was exposed and ligated with an 8-0 suture as previously described. For the WT-Control animals, the corresponding branches of the portal vein were exposed but not ligated.

2.3. Handling of serum samples

At the end of the trial, all animals were anesthetized after overnight fasting, and serum samples were collected and immediately frozen. A total of 250 μL of thawed serum samples and 750 μL of prechilled acetonitrile were transferred to 1.5 mL polypropylene tubes, and the mixture was vortexed for 30 s and allowed to stand for 20 min at 4 °C before use. The samples were centrifuged at 10,000 rpm for 10 min at 4 °C, and the supernatant was transferred into new tubes. Triglyceride (TG) (BC0625, Solarbio, Beijing, China) and glycerol (E1002, Applygen, Beijing, China) levels were determined by using a biochemical analyzer (AU5800, Beckman Coulter, USA) according to the manufacturer's instructions.

2.4. Hematoxylin and eosin (HE) staining

After the mice were sacrificed, liver samples were stored in 10 % formaldehyde solution and embedded in paraffin. Then, the paraffin sections (4 μm) were dewaxed and rehydrated in differential alcohol gradients for subsequent HE staining to observe the histopathological changes using standard light microscopy. HE staining was performed according to the kit's instructions (G1120, Solarbio, Beijing, China).

2.5. RNA extraction

A FastPure Cell/Tissue Total RNA Isolation Kit (RC101, Vazyme, Nanjing, China) was used to extract the total RNA from the liver following the manufacturer's instructions.

2.6. RT–qPCR analysis

Total RNA (500 ng) was reverse transcribed into complementary DNA (cDNA) using HiScript®III RT Strand SuperMix for qPCR (+gDNA wiper) (R323, Vazyme, Nanjing, China). For each mRNA target, upstream and downstream primers were designed. RT–qPCR was performed using ChamQTM Universal SYBR® qPCR Master Mix (Q712, Vazyme, Nanjing, China) on a Qs1 system following the manufacturer's procedure, with GAPDH as the internal reference gene. The primers used in the experiment are listed in Table S1 (Supplementary document 1).

2.7. Immunohistochemistry (IHC) staining

IHC was performed on 5-μm-thick liver sections. Mice were perfused with phosphate buffered saline (PBS) and 4 % paraformaldehyde (PFA), and the liver was removed and fixed in 4 % PFA overnight. After dehydration in an alcohol gradient and clearance with xylene, the livers were embedded in paraffin and sectioned. After the paraffin sections were deparaffinized with xylene, gradient alcohol hydration was performed. EDTA antigen retrieval solution was added, and the sections were heated at 95 °C for 15 min. The sections were then blocked with PBS containing 10 % goat serum and 0.2 % Triton X-100 and incubated with the indicated antibody overnight at 4 °C. After washing with PBS 3

Table 1
The antibodies used in the experiment.

Antibodies	Source/cat. no.	Host	Dilution
NLRP3	Origene (TA379167)	Rabbit	1:100
Caspase-1 p20	Santa Cruz (sc-398715)	Mouse	1:200
GSDMD	ABclonal (A20197)	Rabbit	1:100
Ki67	Abcam (ab16667)	Rabbit	1:200
PCNA	Abcam (ab92552)	Rabbit	1:300
Cyclin D1	Abcam (ab16663)	Rabbit	1:100
CD4	Servicebio (GB15064)	Rabbit	1:400
CD8	Servicebio (GB GB11068)	Rabbit	1:400
Ctss	Bioss (bs-8558R)	Rabbit	1:200
Aif1	Bioss (bs-1363R)	Rabbit	1:200

times, the sections were sequentially incubated with the appropriate biotinylated secondary antibody and avidin-biotin complex for 30 min each. DAB peroxidase substrate was used for development, and the images were captured under a light microscope. The results were analyzed using ImageJ software. The antibodies used in the experiment are listed in Table 1.

2.8. Western blotting (WB)

Livers were collected and stored at −80 °C. The livers were lysed with RIPA lysis buffer and centrifuged, and the supernatant was obtained. The protein concentration was measured using a BCA protein detection kit. Next, the proteins were separated by SDS–PAGE and transferred to Immun-Blot PVDF membranes. The membranes were washed, blocked, and incubated with the primary antibody and then

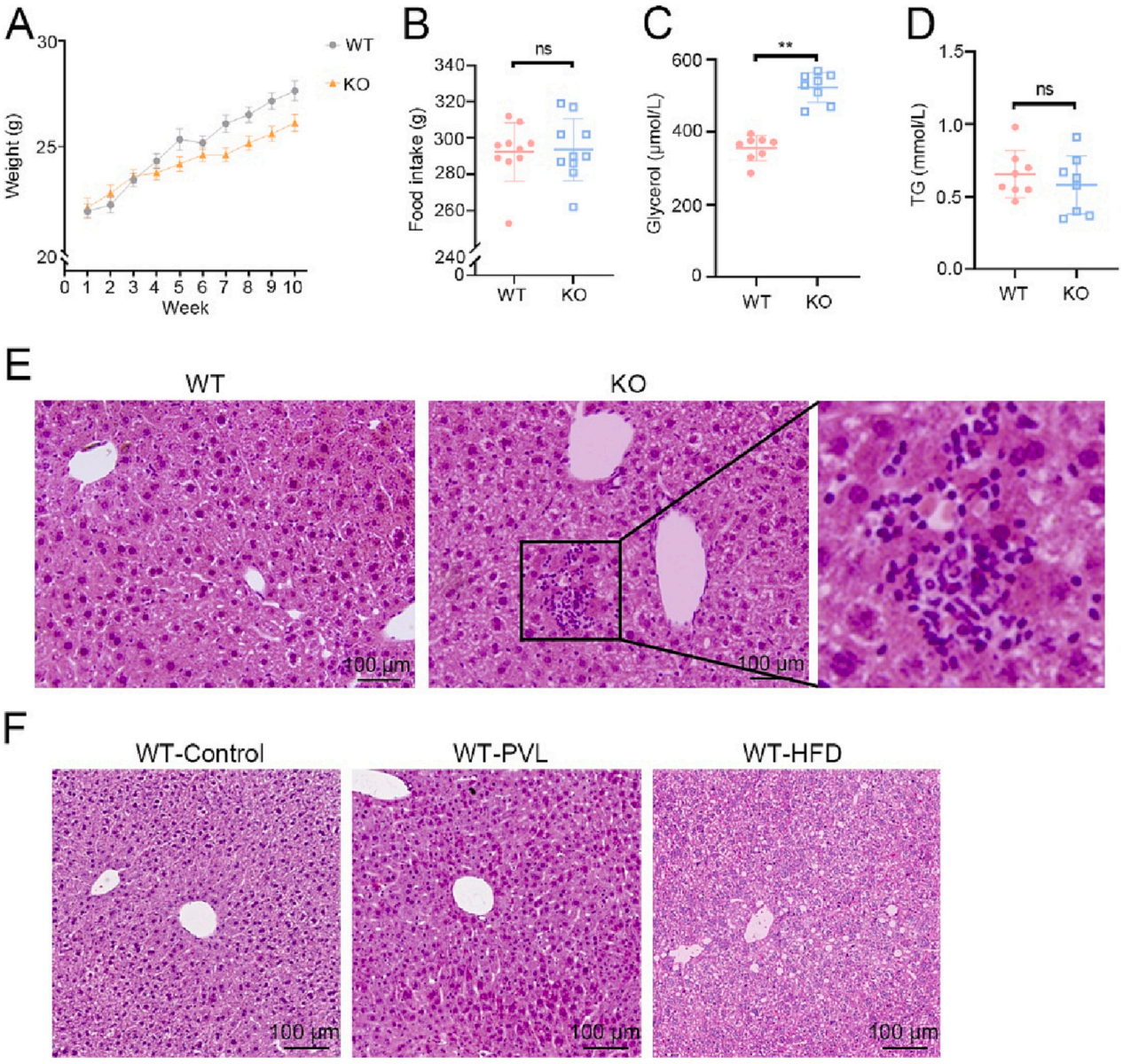

Fig. 1. Phenotypic changes in *Aqp9*$^{-/-}$ mice. A, Weight change curve. Compared with *Aqp9*$^{+/+}$ mice, the body weight of *Aqp9*$^{-/-}$ mice increased slowly. $n = 8$. B, Weekly food intake in each group (8 mice). There was no difference between the two groups. $n = 10$. C, Serum glycerol level. After *Aqp9* knockout, the serum glycerol levels increased. n = 8. D, Serum TG levels. Knockout of *Aqp9* had no significant effect on serum TG levels. n = 8. E, HE staining of liver tissue in the two groups of mice. The liver tissue morphology of the two groups was normal, and the hepatic lobule structure was complete. However, aggregations of basophilic nuclei were observed in the liver tissue of *Aqp9*$^{-/-}$ mice. Black circles indicate a basophilic mass. F, No basophilic mass was found in the liver tissues of the control group and the PVL and NAFLD model groups. The scale is 100 μm. TG, triglyceride; WT, wild-type; KO, knockout; PVL, portal vein ligation; HFD, high-fat diet.

with an appropriate horseradish peroxidase-conjugated secondary antibody (1:5000, goat anti-rabbit or goat anti-mouse; EASYBIO, China). The signal was detected using an enhanced/super ECL kit (DE2002, DiNing, China). The images were scanned, and the relative density of the immunoreactive bands was determined using ImageJ software.

The primary antibodies used in this study are shown below: NLRP3 (1:500, A5652, ABclonal, USA), caspase-1 (1:500, sc-56036, Santa Cruz Biotechnology, USA), GSDMD (1:500, A5652, ABclonal, USA), and β-actin (1:1000, bsm-33036 M, Bioss, China).

2.9. mRNA-seq and sequencing data analysis

Total RNA was extracted using TRIzol reagent (Thermo Fisher, 15596018) according to the manufacturer's instructions. The RNA was quantified by a Bioanalyzer 2100 and RNA 6000 Nano LabChip Kit (Agilent, CA, USA, 5067-1511). RNA samples with RIN > 7.0 were used to construct a sequencing library. The mRNA was purified by using Dynabeads Oligo (dT) (Thermo Fisher, CA, USA) and fragmented into short fragments. Then, the cleaved RNA fragments were reverse-transcribed to generate cDNA by SuperScript™ II Reverse Transcriptase (Invitrogen, cat. 1896649, USA). A cDNA library was sequenced with the Illumina NovaseqTM 6000 sequence platform. The HISAT2 (https://daehwankimlab.github.io/hisat2/, version: hisat2-2.2.1) package was used to align the reference genome. StringTie and Ballgown (http://www.bioconductor.org/packages/release/bioc/html/ballgown.html) were used to estimate the expression levels of all transcripts and perform expression abundance for mRNAs by calculating the FPKM (fragment per kilobase of transcript per million mapped reads) value. Genes with a false discovery rate (FDR) below 0.05 and absolute fold change ≥2 were considered differentially expressed genes. Differentially expressed genes were then subjected to Gene Ontology (GO) enrichment analysis (http://www.geneontology.org/).

2.10. TMT-labeled quantitative proteomics

TMT-labeled quantitative proteomics was completed in cooperation with Shanghai Bioprofile Technology Company Ltd. (Shanghai, China). Liver tissues were suspended on ice in 200 μL lysis buffer. Then, the samples were ultrasonicated. Undissolved cellular debris was removed by centrifugation. The supernatant was collected and the protein concentration was quantified using a BCA Protein Assay Kit. The samples were then subjected to the following steps: protein digestion, TMT labeling of peptides, high pH reversed-phase fractionation (HPRP), LC–MS analysis, database searching, and analysis. Differentially significantly expressed proteins were screened with the cutoff of a ratio fold change of >1.20 or <0.83 and $p < 0.05$. The detailed protocol used for proteomics is described in Text S1 (Supplementary document 1).

2.11. Metabonomics

Metabonomics was completed in cooperation with Shanghai Bioprofile Technology Company Ltd. (Shanghai, China). The changes observed in the metabolites in the liver following knockout of AQP9 were screened using a UPLC-ESI-Q-Orbitrap-MS system (UHPLC, Shimadzu Nexera X2 LC-30AD, Shimadzu, Japan) coupled with Q-Exactive Plus (Thermo Scientific, San Jose, USA). The detailed protocol used for metabonomics is described in Text S2 (Supplementary document 1).

2.12. Statistical analysis

GraphPad Prism version 8.0 was used to analyze the data, and the data are presented in the graphs as the mean ± SEM. The data from the two groups were analyzed by Student's *t*-test (unpaired *t*-test), and $p < 0.05$ was used to determine significant differences. Each experiment was repeated at least three times.

3. Results

3.1. Knockout of Aqp9 reduced body weight by affecting glycerol metabolism, hepatocyte death and inflammatory cell infiltration

To evaluate the phenotypic changes in $Aqp9^{-/-}$ mice, their body weight, serological indicators and liver histomorphological changes were investigated. As shown in Fig. 1A, compared to $Aqp9^{+/+}$ mice, $Aqp9^{-/-}$ mice gained less weight over time. However, there was no difference in weekly food intake between the two groups (Fig. 1B). To determine whether these mice had defects in their glycerol metabolism, we measured their serum glycerol levels. Compared with the $Aqp9^{+/+}$ mice, $Aqp9^{-/-}$ mice exhibited significantly increased serum glycerol levels (Fig. 1C), but there was no significant change in their TG levels (Fig. 1D). HE staining of their liver tissue showed scattered basophilic nuclei in the hepatic lobules (Fig. 1E), which contained dead hepatocytes and inflammatory cells.

To clarify that the scattered basophilic masses in the liver tissue were caused by *Aqp9* knockout, rather than pathological factors, we built NAFLD and PVL models and looked for a basophilic mass. As shown in 1E, no basophilic mass was observed in the NAFLD and PVL models of $Aqp9^{+/+}$ mice.

3.2. Transcriptomics revealed that knockout of Aqp9 triggered immune and inflammatory responses, causing pyroptosis and leading to compensatory proliferation of hepatocytes

A total of 844 differentially expressed genes (DEGs) were identified by transcriptomics, of which 570 were upregulated and 274 were downregulated (Fig. 2A, B). Supplementary document 2 provides detailed information on all DEGs. To explore the mechanisms underlying the hepatocyte death and inflammatory cell infiltration caused by *Aqp9* knockout, we performed GO enrichment analysis on the DEGs, focusing on biological processes. Biological processes were mainly enriched in immune and inflammation-related pathways (Fig. 2C). Knockout of *Aqp9* triggered immune and inflammatory responses in liver tissue. In addition, 26 genes in the cell differentiation pathway were enriched (Fig. 2C), suggesting that cell proliferation, differentiation, and death-related pathways may be initiated. According to the heatmap, 166 genes were upregulated and 7 genes were downregulated in the immune-related pathway, among which a large number of Ighv and Igkv genes were upregulated (Fig. 2D), suggesting that the immune response was activated, immunoglobulin was overexpressed, and antigen binding activity was increased.

Since activation of the body's immune response is often accompanied by inflammation, the DEGs related to inflammation were further investigated. There were 37 upregulated and 4 downregulated inflammation-related genes (Fig. 2E). Chemokine receptors, cytokine production, acyloxyacyl hydrolase and other antiviral or bacterial infections were the main causes of inflammation. In addition, GO analysis also showed enrichment for cell differentiation (Fig. 2C), so we further searched for DEGs related to cell proliferation, differentiation and death. The results showed that 126 genes were upregulated and 34 were downregulated (Fig. 2F). Cell proliferation-related genes mainly include those involved in hepatocyte proliferation (Fgl1), mesenchymal stem cell proliferation (Ccne1), T-cell proliferation (Coro1a, Spn, Anxa1, Aif1, Ccl5, Vcam1), and B-cell proliferation (Ang, Cyba, Lrg1, Itgb3, Jun). The genes related to cell differentiation involves those related to hepatocyte differentiation (Hhex, Anxa1), leukocyte differentiation (Hhex, Spi1), endothelial differentiation (Itgb2, Mmp9, Lama3, Inhba), and lymphocyte differentiation (Plcg2, Cd8a, Tox, Spi1, Gas6, Ihh, Flcn, Fcer1g, Pglyrp1, Cd74). Death-related genes included those related to autophagy (Cdkn2d) and programmed necrosis (Ripk3). Supplementary documents 3, 4, and 5 provide detailed information on the DEGs associated with immunity, inflammation and cell proliferation, differentiation and death.

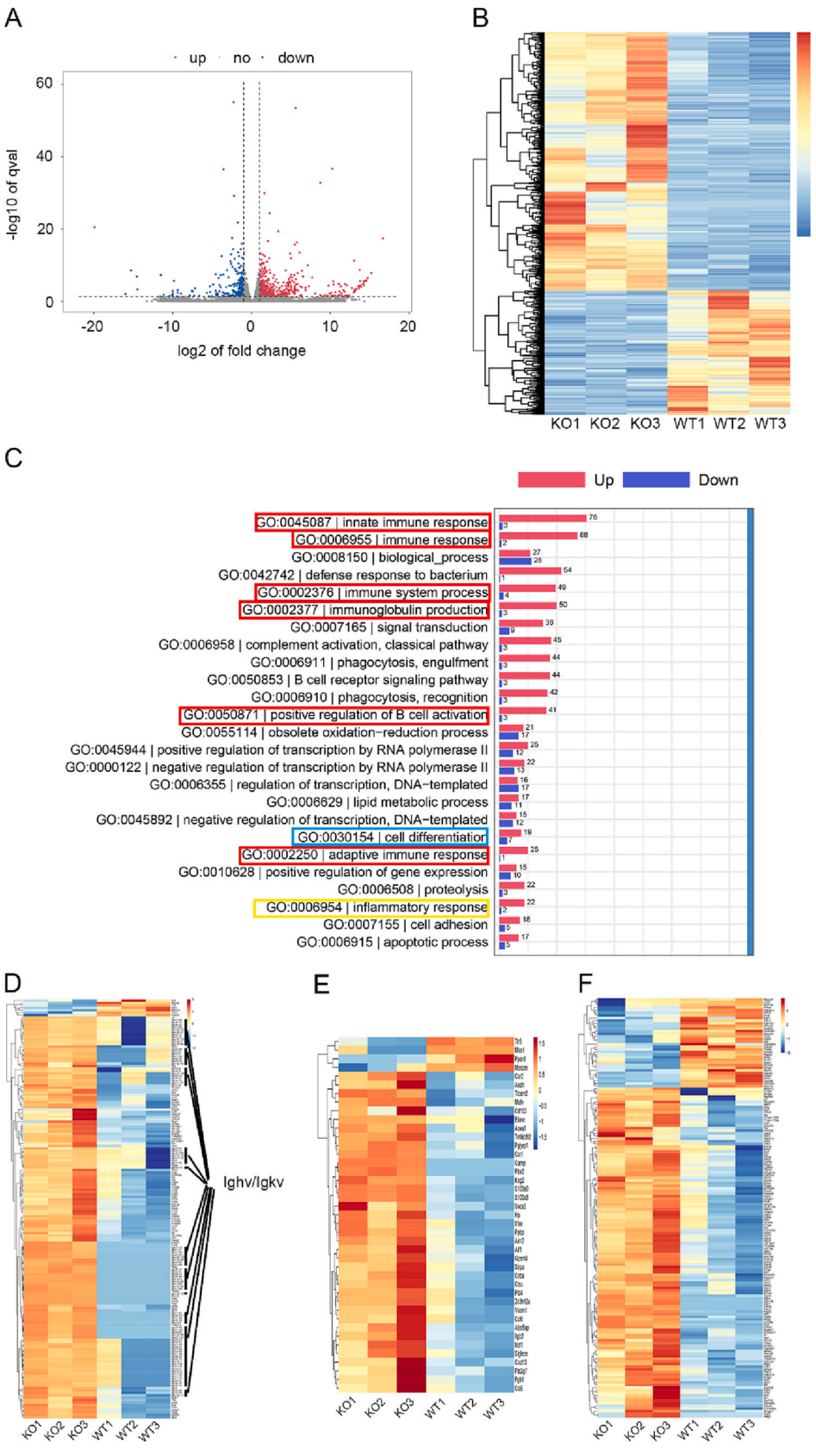

Fig. 2. Transcriptomic alteration. A, Volcano map of DEGs. B, Heatmap of all DEGs. A total of 844 DEGs. C, GO enrichment analysis of the biological processes (top 25). The red boxes indicate immune-related pathways. The yellow box indicates the inflammatory pathway. The blue box indicates the cell differentiation pathway. D, Heatmap of immune-related genes. The DEGs were mainly in the Ighv and Igkv protein families. E, Inflammation-related gene heatmap. F, Cell proliferation-, death- and differentiation-related gene heatmap. WT, wild-type; KO, knockout.

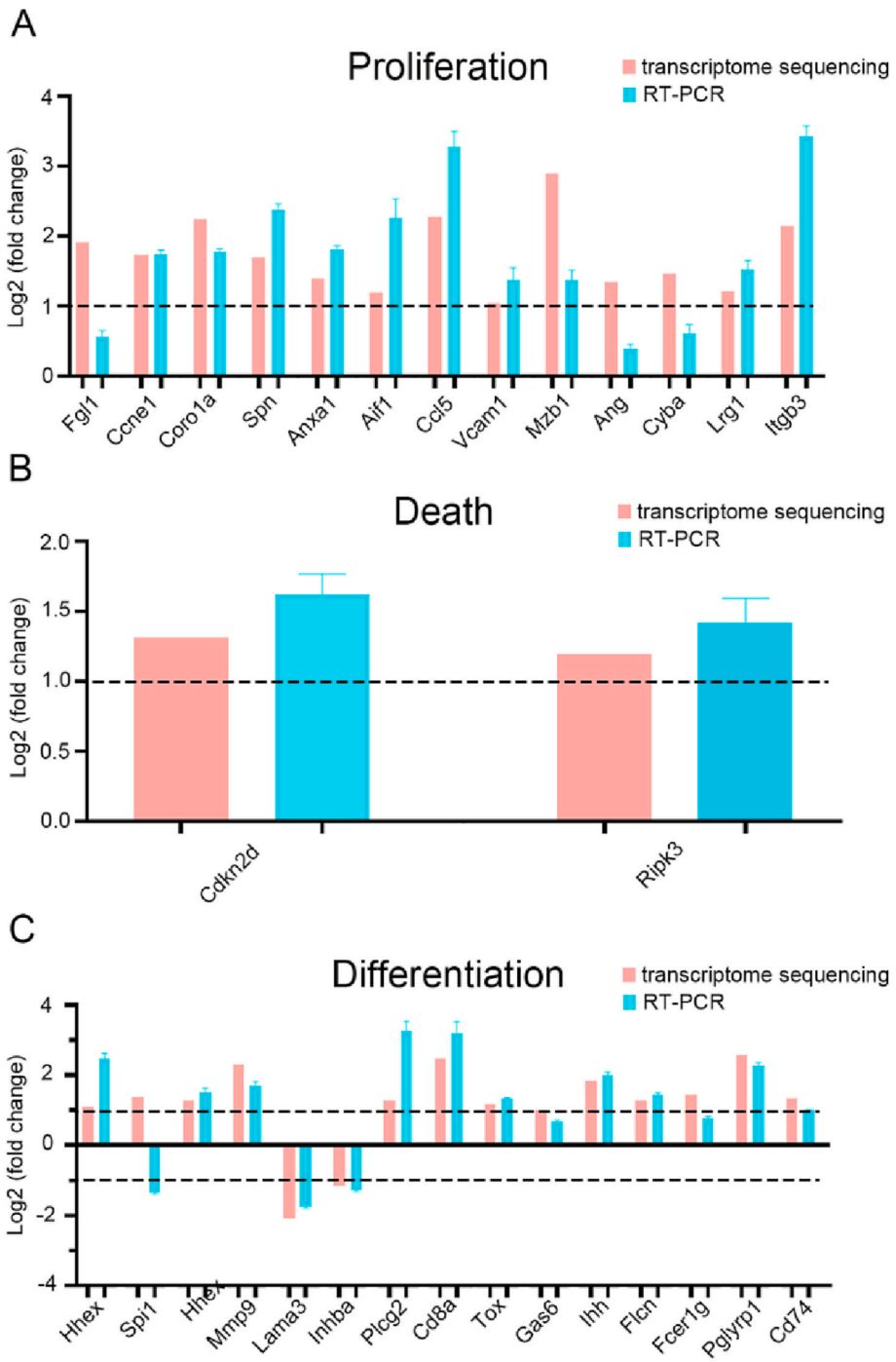

Fig. 3. RT–qPCR verification of some DEGs. A, RT–qPCR verification of some cell proliferation-related genes. B, RT–qPCR verification of cell death-related genes. C, RT–qPCR verification of some cell differentiation-related genes. The RT–qPCR results of all detected DEGs except Spi1 were consistent with the trend of mRNA-seq data.

The RT–qPCR and RNA-seq results were consistent, confirming that cell proliferation and death-related pathways were activated (Fig. 3A, B). Most of the cell differentiation genes were upregulated, but several genes were downregulated, such as the endothelial cell differentiation-related genes Lama3 and Inhba (Fig. 3C).

Transcriptome analysis revealed some molecular changes related to programmed cell death, including Plcg2, Mecom, Lgals3, Cdkn2 d and Ripk3. In addition to the obvious inflammatory reaction, we speculated that the hepatocytes underwent pyroptosis. The IHC results confirmed that liver cell pyroptosis occurred after *Aqp9* knockout (Fig. 4A, C, E). The WB results also showed upregulated expression of pyroptosis core proteins after *Aqp9* knockout (Fig. 4B, D, F).

The IHC staining showed that the expression of Ki67, PCNA and Cyclin D1, the key factors of cell proliferation, was upregulated in *Aqp9*$^{-/-}$ mice (Fig. 5), confirming the compensatory proliferation of hepatocytes after *Aqp9* knockout.

3.3. Proteomics showed that knockout of Aqp9 recruited B cells and CD4^{+} *T cells through upregulated cathepsin S (Ctss) and macrophage activation, inducing immune and inflammatory responses*

A total of 510 differentially expressed proteins (DEPs) were

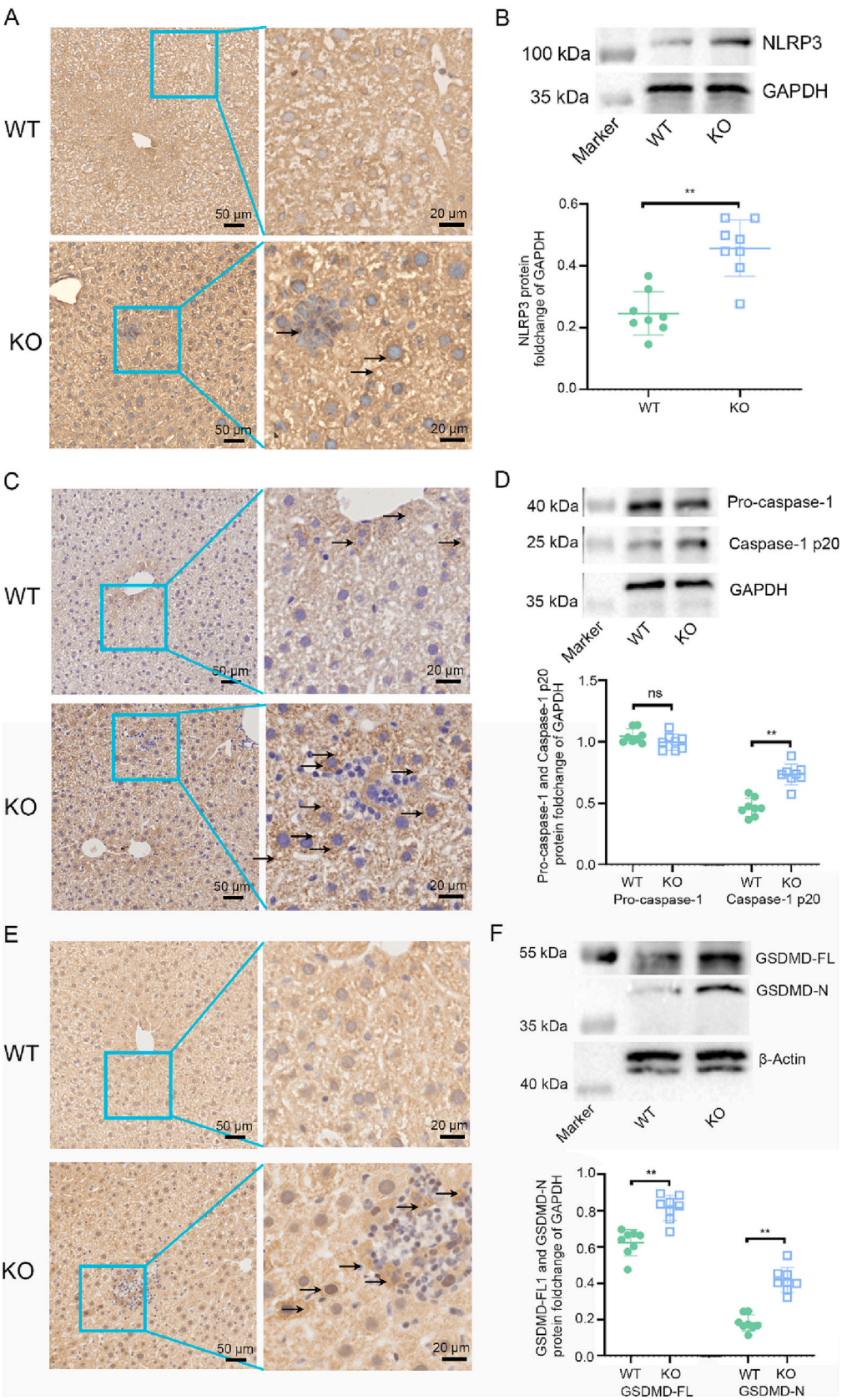

Fig. 4. Changes in the expression of pyroptosis core proteins. A, IHC staining of NLRP3. After Aqp9 knockout, positive brown particles increased in the liver tissue. B, Representative immunoblots of NLRP3 and GAPDH levels in livers. After knockout of *Aqp9*, the expression of NLRP3 increased. C, IHC staining of Caspase-1. The positive particles in *Aqp9*$^{-/-}$ mouse hepatocytes increased. D, Representative immunoblots of Caspase-1 and GAPDH levels in livers. After knockout of *Aqp9*, the expression of Caspase-1 p20, the active fragment of Caspase-1, increased. E, IHC staining of GSDMD (full length + N-terminal). After *Aqp9* knockout, the cells with increased expression of GSDMD-positive particles were mainly concentrated in or around the basophilic mass. F, Representative immunoblots of GSDMD and β-Actin levels in livers. After knockout of *Aqp9*, the expression of GSDMD-N, the active fragment of Caspase-1, increased. The right column is the enlarged image in the blue box in the left column. The left column scale bar is 50 μm. The right column scale bar is 20 μm. WT, wild-type; KO, knockout.

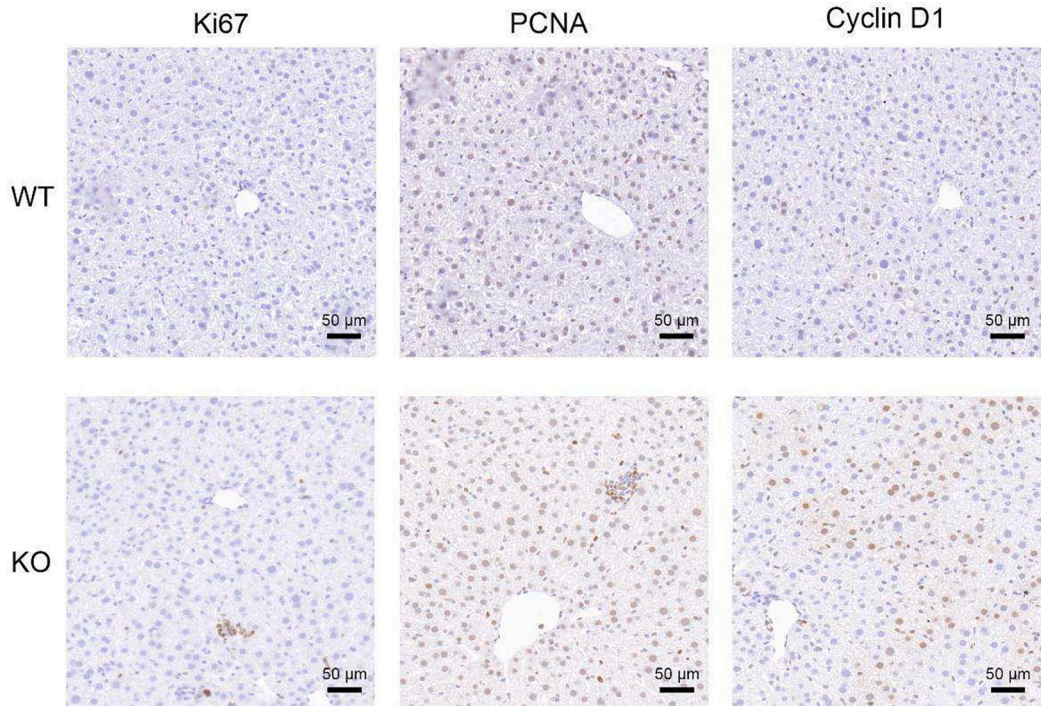

Fig. 5. IHC staining of proliferation-related indicators. Ki67 is mainly concentrated in the basophilic mass of *Aqp9*$^{-/-}$ mice. PCNA-positive cells showed a diffuse increase after *Aqp9* knockout. Cyclin D1-positive cells showed a scattered increase after *Aqp9* knockout. The scale bar is 50 μm. WT, wild-type; KO, knockout.

identified by proteomics, of which 299 were upregulated and 211 were downregulated (Fig. 6A, B). Supplementary document 6 provides detailed information on all DEPs.

To further clarify the specific immune and inflammatory pathways triggered by *Aqp9* knockout, 173 immune and 41 inflammation-related DEGs were screened out from 510 DEPs. As shown in Fig. 6C, eight immune-related genes were screened, namely, Igkv15-103, Igkv17-121, Ctss, Fcer1g, S100a9, S100a8, Enpp1 and Igkv2-112. As shown in Fig. 6D, seven inflammation-related genes were screened out, namely, Cd163, Ctss, Aif1, S100a9, S100a8, Alox5ap and Itgb2. Igkv and Ctss were among the identified genes. Igkv is an immunoglobulin gene that is mainly involved in the activation of B cells. Ctss regulates antigen processing and communication with T cells to recruit B cells [16]. Studies have shown that Ctss activates CD4$^+$ T cells but not CD8$^+$ T cells [16]. Therefore, we used IHC to detect the expression of CD4, CD8 and Ctss. As shown in Fig. 7A and B, CD4$^+$ T-cell aggregation was present in the basophilic mass of *Aqp9*$^{-/-}$ mice, but no CD8$^+$ T-cell aggregation was observed. After knocking out *Aqp9*, the expression of Ctss was significantly upregulated (Fig. 7C).

We further screened genes related to cell proliferation, differentiation and death among the DEPs. As shown in Fig. 6E, a total of 9 genes were identified, namely, Cyp7b1, Itgb3, Hcls1, Itgb2, Fcer1g, Aif1, Enpp1, S100a11, and Rbp1. Combined with inflammatory genes, Aif1, Itgb2 and S100a11 may play an important role in the interested pathways. Aif1 is a marker of macrophages and microglia. The upregulated expression of Aif1 in the liver represents the activation of macrophages. Igtb2 is also closely related to T-cell proliferation and leukocyte migration and aggregation. IHC also confirmed the increased expression levels of Aif1 in *Aqp9*$^{-/-}$ mouse livers (Fig. 7D). Moreover, S100a11 promotes inflammation and cell proliferation.

In summary, the proteomics analysis revealed that knockout of *Aqp9* upregulated the expression of Ctss, recruited B cells and CD4$^+$ T cells, and activated macrophages to induce immune and inflammatory responses.

3.4. Metabolomics revealed that cAMP levels were increased after Aqp9 knockout, suggesting that the self-feedback mechanism inhibiting the liver immune response was activated

A total of 185 compounds were screened, including 111 in positive ion mode (Fig. 8A) and 74 in negative ion mode (Fig. 8B). Supplementary document 7 provides detailed information on all of the differential metabolites. The differential metabolites were analyzed by KEGG and found to be enriched in glycerol metabolism-related pathways (Fig. 8C), which further indicated that knockout of *Aqp9* caused a liver glycerol metabolism disorder at the metabolomics level. In addition, the cyclic adenosine monophosphate (cAMP) signaling pathway was also enriched (Fig. 8C), and cAMP levels was significantly increased in *Aqp9*$^{-/-}$ mice (Fig. 8D). In normal tissues, an activated immune response can trigger the immunosuppressive effect of extracellular adenosine, thereby increasing intracellular cAMP levels. cAMP protects against acute inflammatory injury in vivo by inhibiting the production of proinflammatory cytokines and suppressing activated immune cells and tissues [17]. In addition, the metabolomics analysis also found an enriched cell cycle-related metabolite and decreased levels of coenzyme A, suggesting cell death or compensatory proliferation.

4. Discussion

In this study, *Aqp9* knockout mice were used to explore the mechanism by which AQP9 maintains the physiological status of the liver. With their unique glycerol transport capacity, AQP channels play a key role in osmotic regulation and energy metabolism by controlling intracellular glycerol concentrations [18]. By controlling glycerol levels in the liver, fat, epidermis, and other tissues, AQP channels are involved in skin hydration, cell proliferation, fat metabolism, and cancer pathogenesis [19]. AQP channels can also specifically promote the transmembrane transport of arsenite, for which AQP9 has the highest permeability. The expression of AQP9 in leukocytes facilitates arsenic trioxide transport, allowing the compound to be used as an antitumor chemotherapy drug [20]. Due to the prevalence and importance of

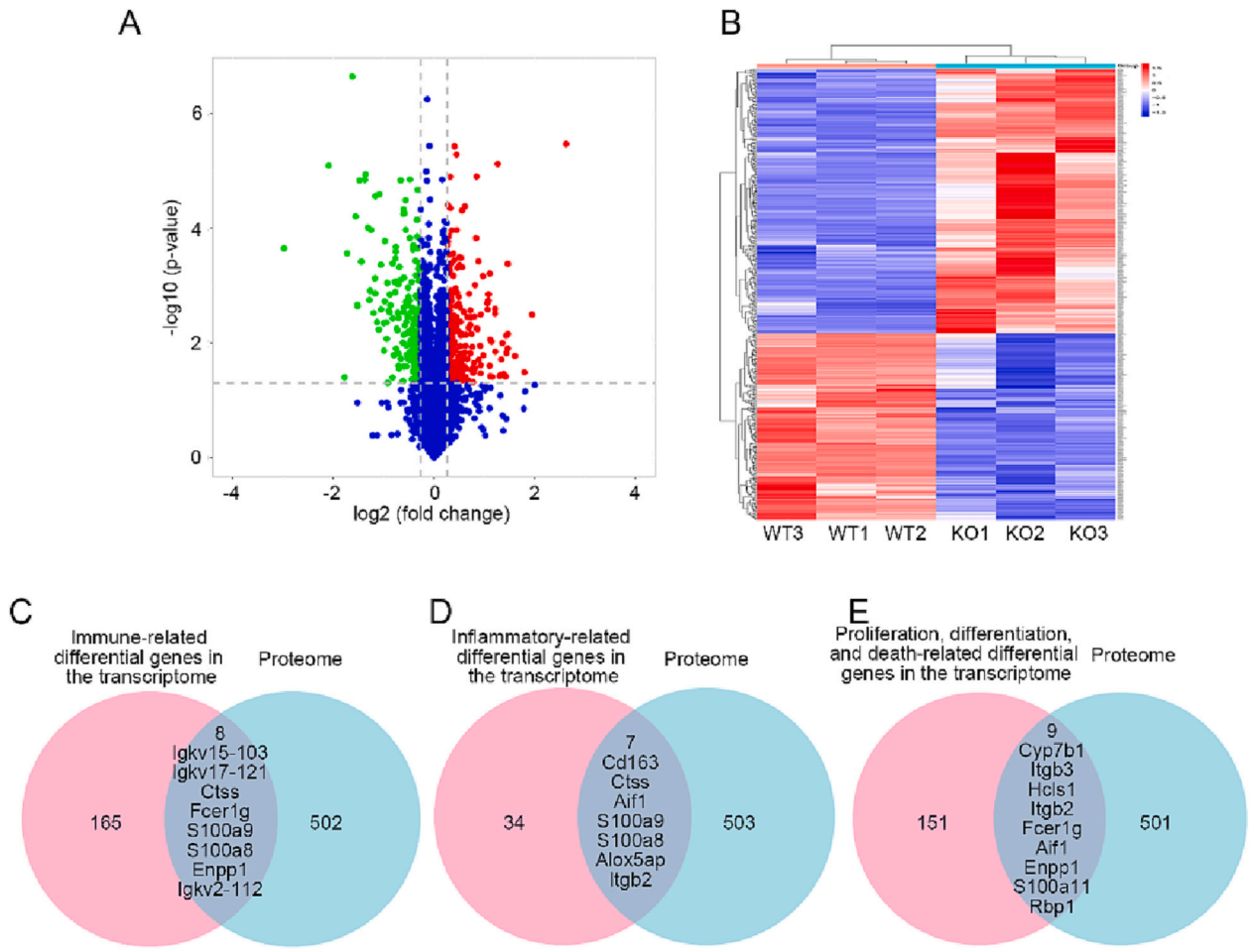

Fig. 6. Proteomic alteration. A, DEP volcano plot. B, Heatmaps of all DEPs. A total of 510 DEPs. C, DEGs associated with immunity screened by transcriptomics and proteomics. D, DEGs associated with inflammation screened by transcriptomics and proteomics. E, DEGs related to cell proliferation, death and differentiation were screened by transcriptomics and proteomics. WT, wild-type; KO, knockout.

AQP9, it is particularly important to study its physiological role in normal liver tissue to obtain an in-depth understanding of its mechanism of action in different liver diseases.

The liver is responsible for glycerol metabolism. AQP9 is the main water glycerol channel in the liver, and it is also the main channel by which glycerol enters the liver. Adipose tissue decomposes TG to generate glycerol, which is released into the blood by AQP7. After the blood reaches the liver tissue, glycerol is transported by AQP9 into the liver cells, and then glycerol is phosphorylated to form glycerol-3-phosphate [3]. The body preferentially engages in gluconeogenesis when it is in a fasting state and breaks down TG when it is in a postmeal state [5]. Compared to *Aqp9*$^{+/+}$ mice, *Aqp9*$^{-/-}$ mice did not exhibit increased hepatic glucose output after glycerol infusion [21]. This finding suggests that AQP9 plays a key role in glycerol transport during gluconeogenesis. Glycerol permeability of hepatocytes is mainly affected by plasma membrane AQP9 abundance. In obese type II diabetic mice, downregulated AQP9 expression improved their diabetes status, suggesting that reduced liver glycerol uptake suppressed gluconeogenesis [22]. Thus, AQP9 is involved not only in glycerol and glucose metabolism but also in the occurrence and development of diabetes, and AQP9 can be used as a potential therapeutic target for liver-related diseases. In this study, we found that AQP9 is critical for the maintenance of normal body weight. The weight gain of *Aqp9*$^{-/-}$ mice was slow, and their serum glycerol levels increased, indicating that AQP9 knockout disrupted glycerol metabolism. However, there was no significant change in TG levels. TG in the blood is derived from its synthesis in liver cells and intestinal epithelial cells. After knockout of *Aqp9*, although the ability of hepatocytes to synthesize TG was weakened, TG synthesis by intestinal mucosal epithelial cells was compensatorily increased, which may be the main reason why normal serum TG levels were maintained in these mice. Rojek et al. also found that serum glycerol levels were elevated in *Aqp9*$^{-/-}$ mice. In contrast to our results, the mouse TG levels were elevated in their experiment [21]. This contradiction may be due to the different levels in the compensatory increase in TG synthesized by intestinal epithelial cells caused by different feeding environments and diets.

This study found that after the knockout of *Aqp9*, basophilic masses formed and were scattered in the liver tissue, and they contained dead liver and inflammatory cells. To explore the downstream pathway changes induced by knockout of *Aqp9*, and the physiological pathways in which AQP9 is involved, we used a combined analysis of transcriptomics, proteomics and metabolomics to screen DEGs. GO enrichment of 851 DEGs screened by transcriptomics showed that they were mainly enriched in immune- and inflammation-related pathways and immunoglobulin-related genes. In addition, DEGs related to cell proliferation, differentiation and death were screened. Proteomics further narrowed the range of the DEGs, and 12 immune- and inflammation-related genes were screened out, namely, Igkv2-112, Igkv15-103, Igkv17-121, S100a9, S100a8, Itgb2, Ctss, Fcer1g, Enpp1, Cd163, Aif1, and Alox5ap. Igkv is an immunoglobulin gene that is mainly involved in the activation of B cells. Ctss is recognized as a member of the proteolytic cocktail within the lysosome, which degrades damaged proteins. However, an increasing number of studies have shown that it has additional functions, including antigen processing and antigen

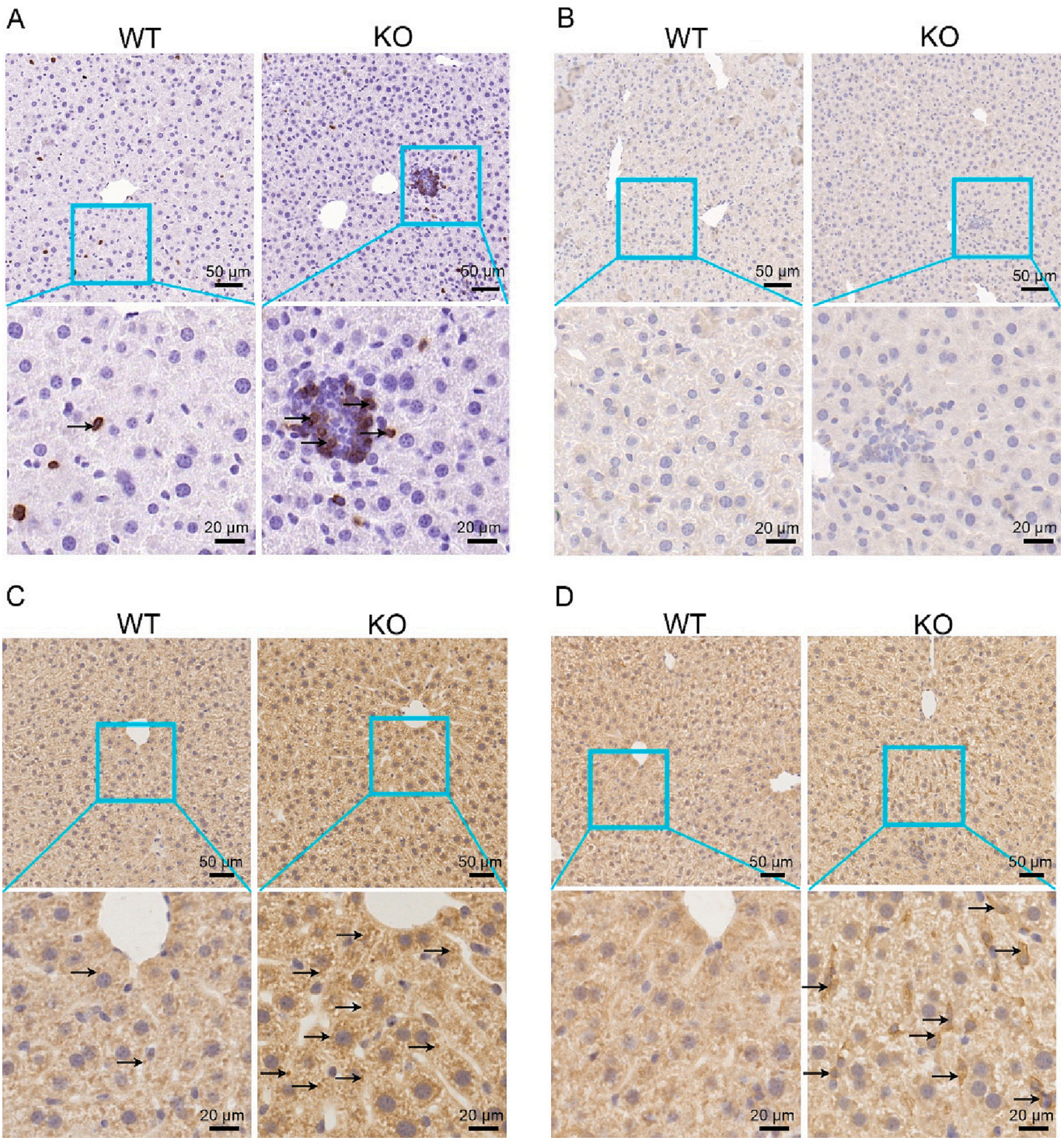

Fig. 7. IHC staining of representative DEPs. A, CD4 expression changes. In *Aqp9*$^{-/-}$ mice, CD4^{+} T cells accumulate in the basophilic clusters. B, CD8 detection. No obvious positive cells were found in the liver tissues of either group. C, Expression changes of Ctss. Ctss expression was significantly increased after *Aqp9* knockout. D, Expression changes of Aif1. After *Aqp9* knockout, the number of positive cells increased significantly. The lower row is an enlarged image from the blue box in the upper row. The upper image scale bar is 50 μm, and the lower image scale bar is 20 μm. WT, wild-type; KO, knockout.

presentation, and it can process invariant strands/CD74 to promote major histocompatibility complex class II (MHC-II) antigen presentation, which in turn induces CD4^{+} T cells [16,23,24]. Studies have confirmed that B cells rely on the activity of Ctss to maintain communication with CD4^{+} T cells and limit the recognition of CD8^{+} T cells to recruit B cells [16,24]. The IHC results also confirmed that there were a large number of CD4^{+} T cells in the basophilic masses in *Aqp9*$^{-/-}$ mouse liver tissue, but no CD8^{+} T cells were found. In addition, upregulated S100a8 and S100a9 activate inflammatory cells and cytokines primarily through the chemotaxis of neutrophils [25]. This part of the experiment confirmed that *Aqp9* knockout can induce an immune response in liver tissue; that is, AQP9 can inhibit excessive immune responses to maintain the normal physiological state of liver tissue. However, Cui et al. reported that IL-7 induces AQP9 expression in CD8^{+} T cells and promotes glycerol input and TAG synthesis, which are essential for CD8^{+} T-cell survival and homeostasis [25]. That is, the expression of AQP9 can

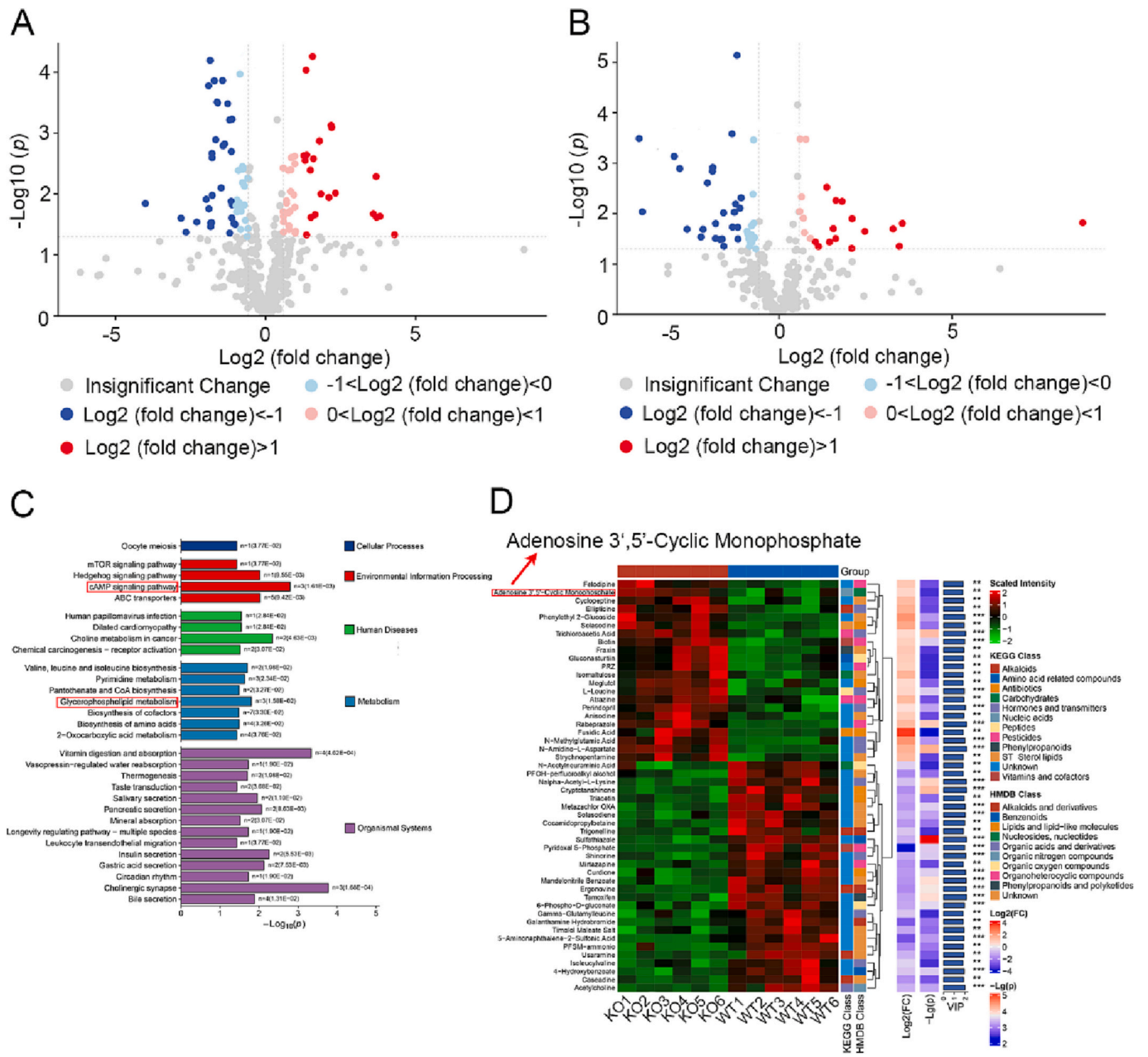

Fig. 8. Metabolomic alteration. A, Volcano diagram of differential metabolites screened by positive ion mode. There were 111 differential metabolites. B, Volcano diagram of differential metabolites screened by negative ion mode. There were 74 differential metabolites. C, KEGG enrichment analysis of differential metabolites. The red boxes identify glycerophospholipid metabolism and cAMP signaling pathways. D, Complex heatmap of the 50 most significantly different metabolites. The red box indicates cAMP. WT, wild-type; KO, knockout.

maintain the immune function of $CD8^+$ T cells. This finding is contrary to what we found in the *Aqp9* knockout-induced immune response. We have demonstrated that knockout of *Aqp9* recruits $CD4^+$ T cells rather than $CD8^+$ T cells, indicating that AQP9 expression can inhibit the function of $CD4^+$ T cells. Combined with the findings of Cui et al., AQP9 can inhibit the immune function of $CD4^+$ T cells and maintain the immune function of $CD8^+$ T cells. In mice with bacterial endotoxin-induced sepsis, gene deletion of *Aqp9* alleviated oxidative stress and improved survival [26], whereas our study found that physiological *Aqp9* knockout induces inflammation. This contradiction is because knockout of *Aqp9* in septic mice reduced the activity of $CD8^+$ T cells, while knockout in healthy mice activated $CD4^+$ T cells.

Immune and inflammatory responses induced by *Aqp9* knockout can trigger mild pyroptosis in liver tissue. Transcriptomics and experiments confirmed that *Aqp9* knockout caused scattered pyroptosis in liver tissue. However, AQP9 inhibitors significantly reduced NLRP3 activation in the heart and kidney of septic mice [27]. Our previous study found that knockout of *Aqp9* reduced CCl_4-induced chronic liver injury in a mouse model because knockout of Aqp9 attenuated lipid peroxidation in hepatocytes [25]. We found that the immune inflammation induced by knockout of *Aqp9* in the physiological state triggered pyroptosis. The activation of NLRP3 and oxidative stress by AQP9 in the pathological state may be realized through the $CD8^+$ T-cell-mediated inflammatory response. However, AQP9 in the physiologically healthy state can inhibit inflammation by suppressing the activation of $CD4^+$ T cells. This result reveals that the effect of AQP9 on lipid metabolism under physiological conditions can be compensated by other pathways, but it is crucial for the maintenance of the liver immune response.

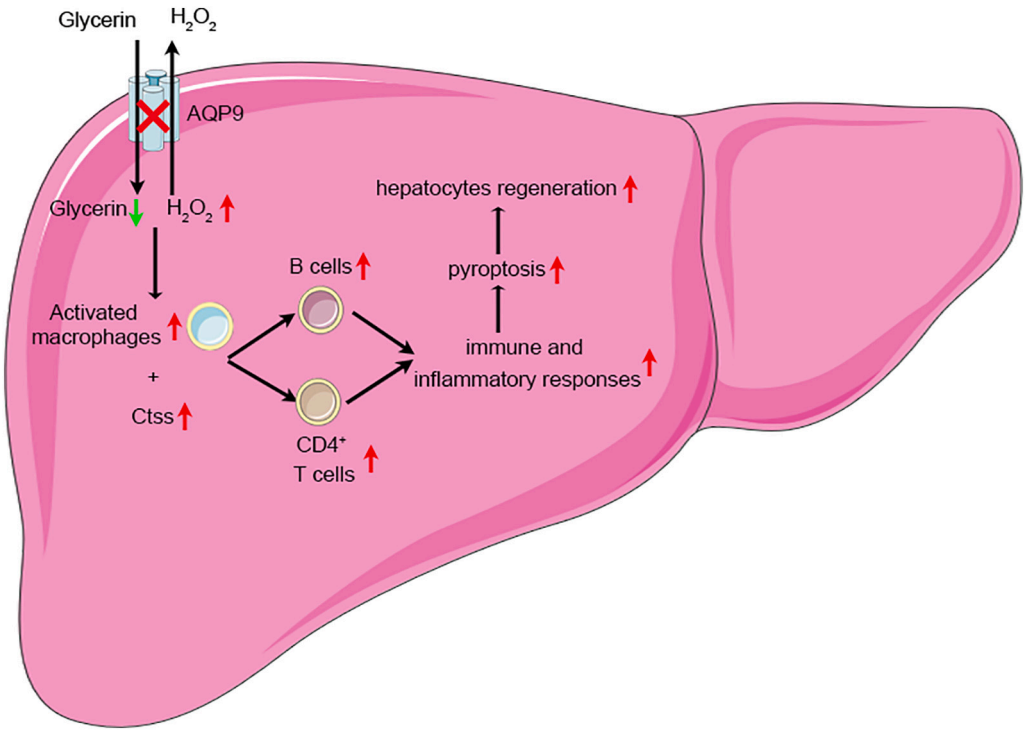

Fig. 9. Schematic summary of liver physiological function in *Aqp9* gene knockout mice.

We further screened genes related to cell proliferation, differentiation and death. A total of 9 genes were identified, namely, Cyp7b1, Itgb3, Hcls1, Itgb2, Fcer1g, Aif1, Enpp1, S100a11, and Rbp1. Aif1, or Iba1, is a marker of microglia and macrophages. The expression of Aif1 in the liver tissue of $Aqp9^{-/-}$ mice was upregulated, indicating that macrophages were activated. Studies of Aif1 and S100a11 in hepatocellular carcinoma have shown that both promote the progression of hepatocellular carcinoma [28,29]. Macrophage Aif1 promotes hepatocyte proliferation by changing the tumor microenvironment [28]. Overexpression of S100a11 in hepatocytes increases inflammation and tumor proliferation, and it also promotes the transformation of hepatocyte steatosis into steatohepatitis, liver fibrosis, and liver cancer [29].

Recent studies have shown that the ubiquitous purine nucleoside adenosine physiologically inhibits activated immune cells and protects tissues from acute inflammatory injury in vivo. Extracellular adenosine accumulated in the inflammatory area of the damaged microenvironment first identifies excessive immune damage and then prevents this excessive damage by inhibiting activated immune cells. Extracellular adenosine acts on A2A adenosine receptors to increase intracellular cAMP levels through delayed negative feedback and then inhibits the production of proinflammatory cytokines [30]. The metabolomics analysis found that cAMP levels were increased in $Aqp9^{-/-}$ mice, revealing that healthy tissues can play a protective role through the body's feedback mechanism during inflammation after *Aqp9* knockout.

5. Conclusion

In summary, as shown in Fig. 9, knockout of *Aqp9* recruits B cells and $CD4^+$ T cells through upregulated Ctss and macrophage activation, inducing immune and inflammatory responses. Inflammation is enhanced by the chemotaxis of S100a8 and S100a9 to neutrophils. The immune inflammatory response leads to pyroptosis of hepatocytes, accompanied by the compensatory regeneration of hepatocytes. The findings of this study suggest that AQP9 is essential for the maintenance of liver immune function in the physiological state. Additional studies using *Aqp9* knockout mice will help deepen the understanding of the role of AQP9 in physiological and pathological conditions.

Supplementary data to this article can be found online at https://doi.org/10.1016/j.ijbiomac.2023.125459.

Funding

This work was supported by the Beijing Municipal Natural Science Foundation (No. 7162098) and Beijing Municipal Natural Science Foundation (No. 7232090).

CRediT authorship contribution statement

Q.C., J.Z., Y.X, C.C, W.Z. designed the study; Q.C., J.Z., Z.W. and H.D. carried out experiments; Q.C., M.L., and R.L. analyzed the data; J.F. and J.M. made the figures; Q.C., J.W., X.F, H. L, and X.L. drafted and revised the paper; all authors approved the final version of the manuscript.

Declaration of competing interest

The authors declare that they have no known competing financial interests or personal relationships that could have appeared to influence the work reported in this paper.

Data availability

The datasets used and/or analyzed during the current study are included in this article and its supplementary information files. The datasets are available from the corresponding author on reasonable request.

Acknowledgments

We thank Jiye Hou and Kaixin Zhong at Shanghai Bioprofile Technology Company Ltd. for their technical support in proteomics and metabonomics.

References

[1] N. Maeda, Implications of aquaglyceroporins 7 and 9 in glycerol metabolism and metabolic syndrome, Mol. Asp. Med. 33 (5–6) (2012) 665–675.
[2] C. Zhu, Z. Chen, Z. Jiang, Expression, distribution and role of aquaporin water channels in human and animal stomach and intestines, Int. J. Mol. Sci. 17 (9) (2016).
[3] J. Lebeck, Metabolic impact of the glycerol channels AQP7 and AQP9 in adipose tissue and liver, J. Mol. Endocrinol. 52 (2) (2014) R165–R178.
[4] C. Cai, C. Wang, W. Ji, et al., Knockdown of hepatic aquaglyceroporin-9 alleviates high fat diet-induced non-alcoholic fatty liver disease in rats, Int. Immunopharmacol. 15 (3) (2013) 550–556.
[5] L. Mendez-Gimenez, A. Rodriguez, I. Balaguer, et al., Role of aquaglyceroporins and caveolins in energy and metabolic homeostasis, Mol. Cell. Endocrinol. 397 (1–2) (2014) 78–92.
[6] S. Hirako, Y. Wakayama, H. Kim, et al., The relationship between aquaglyceroporin expression and development of fatty liver in diet-induced obesity and ob/ob mice, Obes. Res. Clin. Pract. 10 (6) (2016) 710–718.
[7] C. Wang, Z.L. Lv, Y.J. Kang, et al., Aquaporin-9 downregulation prevents steatosis in oleic acid-induced non-alcoholic fatty liver disease cell models, Int. J. Mol. Med. 32 (5) (2013) 1159–1165.
[8] P. Gena, M. Mastrodonato, P. Portincasa, et al., Liver glycerol permeability and aquaporin-9 are dysregulated in a murine model of non-alcoholic fatty liver disease, PLoS One 8 (10) (2013), e78139.
[9] A. Rodriguez, P. Gena, L. Mendez-Gimenez, et al., Reduced hepatic aquaporin-9 and glycerol permeability are related to insulin resistance in non-alcoholic fatty liver disease, Int. J. Obes. 38 (9) (2014) 1213–1220.
[10] F. Baldini, P. Portincasa, E. Grasselli, et al., Aquaporin-9 is involved in the lipid-lowering activity of the nutraceutical silybin on hepatocytes through modulation of autophagy and lipid droplets composition, Biochim. Biophys. Acta Mol. Cell Biol. Lipids 1865 (3) (2020), 158586.
[11] Q. Cheng, H. Ding, J. Fang, et al., Aquaporin 9 represents a novel target of chronic liver injury that may antagonize its progression by reducing lipotoxicity, Oxidative Med. Cell. Longev. 2021 (2021), 5653700.
[12] G. Calamita, P. Gena, D. Ferri, et al., Biophysical assessment of aquaporin-9 as principal facilitative pathway in mouse liver import of glucogenetic glycerol, Biol. Cell. 104 (6) (2012) 342–351.
[13] B. Zhang, D. Lv, Y. Chen, et al., Aquaporin-9 facilitates liver regeneration following hepatectomy, Redox Biol. 50 (2022), 102246.
[14] A. Sathyanarayanan, R. Gupta, E.W. Thompson, et al., A comparative study of multi-omics integration tools for cancer driver gene identification and tumour subtyping, Brief. Bioinform. 21 (6) (2020) 1920–1936.
[15] S. Zhang, J. Zhang, Y. An, et al., Multi-omics approaches identify SF3B3 and SIRT3 as candidate autophagic regulators and druggable targets in invasive breast carcinoma, Acta Pharm. Sin. B 11 (5) (2021) 1227–1245.
[16] E. Dheilly, E. Battistello, N. Katanayeva, et al., Cathepsin S regulates antigen processing and T cell activity in non-Hodgkin lymphoma, Cancer Cell 37 (5) (2020) 674–689 e612.
[17] M.V. Sitkovsky, D. Lukashev, S. Apasov, et al., Physiological control of immune response and inflammatory tissue damage by hypoxia-inducible factors and adenosine A2A receptors, Annu. Rev. Immunol. 22 (2004) 657–682.
[18] A. Madeira, T.F. Moura, G. Soveral, Aquaglyceroporins: implications in adipose biology and obesity, Cell. Mol. Life Sci. 72 (4) (2015) 759–771.
[19] A. Rodriguez, V. Catalan, J. Gomez-Ambrosi, et al., Insulin- and leptin-mediated control of aquaglyceroporins in human adipocytes and hepatocytes is mediated via the PI3K/Akt/mTOR signaling cascade, J. Clin. Endocrinol. Metab. 96 (4) (2011) E586–E597.
[20] X. Geng, J. McDermott, J. Lundgren, et al., Role of AQP9 in transport of monomethyselenic acid and selenite, Biometals 30 (5) (2017) 747–755.
[21] A.M. Rojek, M.T. Skowronski, E.M. Fuchtbauer, et al., Defective glycerol metabolism in aquaporin 9 (AQP9) knockout mice, Proc. Natl. Acad. Sci. U. S. A. 104 (9) (2007) 3609–3614.
[22] S.J. Wacker, C. Aponte-Santamaría, P. Kjellbom, et al., The identification of novel, high affinity AQP9 inhibitors in an intracellular binding site, Mol. Membr. Biol. 30 (3) (2013) 246–260.
[23] P. Smyth, J. Sasiwachirangkul, R. Williams, et al., Cathepsin S (CTSS) activity in health and disease - a treasure trove of untapped clinical potential, Mol. Asp. Med. 88 (2022), 101106.
[24] K.V. Rupanagudi, O.P. Kulkarni, J. Lichtnekert, et al., Cathepsin S inhibition suppresses systemic lupus erythematosus and lupus nephritis because cathepsin S is essential for MHC class II-mediated CD4 T cell and B cell priming, Ann. Rheum. Dis. 74 (2) (2015) 452–463.
[25] H.C. Volz, D. Laohachewin, C. Seidel, et al., S100A8/A9 aggravates post-ischemic heart failure through activation of RAGE-dependent NF-kappaB signaling, Basic Res. Cardiol. 107 (2) (2012) 250.
[26] A. Tesse, P. Gena, M. Rutzler, et al., Ablation of aquaporin-9 ameliorates the systemic inflammatory response of LPS-induced endotoxic shock in mouse, Cells 10 (2) (2021).
[27] S. Mohammad, C.E. O'Riordan, C. Verra, et al., RG100204, a novel aquaporin-9 inhibitor, reduces septic cardiomyopathy and multiple organ failure in murine sepsis, Front. Immunol. 13 (2022), 900906.
[28] H. Cai, X.D. Zhu, J.Y. Ao, et al., Colony-stimulating factor-1-induced AIF1 expression in tumor-associated macrophages enhances the progression of hepatocellular carcinoma, Oncoimmunology 6 (9) (2017), e1333213.
[29] C. Sobolewski, D. Abegg, F. Berthou, et al., S100A11/ANXA2 belongs to a tumour suppressor/oncogene network deregulated early with steatosis and involved in inflammation and hepatocellular carcinoma development, Gut 69 (10) (2020) 1841–1854.
[30] Q. Xiao, X. Han, G. Liu, et al., Adenosine restrains ILC2-driven allergic airway inflammation via A2A receptor, Mucosal Immunol. 15 (2) (2022) 338–350.